Earth Planets Space, **61**, 439–445, 2009

Relative effects of electric field and neutral wind on positive ionospheric storms

N. Balan[1]*, H. Alleyne[1], Y. Otsuka[2], D. Vijaya Lekshmi[3], B. G. Fejer[4], and I. McCrea[5]

[1]*Control and Systems Engineering, University of Sheffield, Sheffield S1 3JD, UK*
[2]*Solar-Terrestrial Environment Laboratory, Nagoya University, Aichi 442-8507, Japan*
[3]*Department of Physics, University of Kerala, Trivandrum 695581, India*
[4]*Center for Atmospheric and Space Sciences, Utah State University, Utah 84322-0500, USA*
[5]*Rutherford Appleton Laboratory, Didcot OX11 0QX, UK*

(Received September 6, 2007; Revised January 30, 2008; Accepted February 1, 2008; Online published May 14, 2009)

The paper studies the relative importance of penetrating eastward electric field (PEEF) and direct effects of equatorward neutral wind in leading to positive ionospheric storms at low-mid latitudes using observations and modeling. The observations show strong positive ionospheric storms in total electron content (TEC) and peak electron density (N_{max}) at low-mid latitudes in Japan longitudes (≈125°E–145°E) during the first main phase (started at sunrise on 08 November) of a super double geomagnetic storm during 07–11 November 2004. The model results obtained using the Sheffield University Plasmashpere Ionosphere Model (SUPIM) show that the direct effects of storm-time equatorward neutral wind (that reduce poleward plasma flow and raise the ionosphere to high altitudes of reduced chemical loss) can be the main driver of positive ionospheric storms at low-mid latitudes except in N_{max} around the equator. The equatorward wind without PEEF can also result in stronger positive ionospheric storms than with PEEF. Though PEEF on its own is unlikely to cause positive ionospheric storms, it can lead to positive ionospheric storms in the presence of an equatorward wind.
Key words: Ionospheric storms, electric field, neutral wind.

1. Introduction

Following geomagnetic storms, the ionospheric peak electron density (N_{max}) and total electron content (TEC) often increase/decrease very much from their quiet-time levels. These increase/decrease are known as positive/negative ionospheric storms (e.g., Matsushita, 1959; Matuura, 1972), which are found to depend on time of the day, longitude and season (e.g., Balan and Rao, 1990). Review articles on ionospheric storms are presented by Rishbeth (1991), Prolss (1995) and Abdu (1997). The negative ionospheric storms at mid latitudes are more or less understood in terms of the upwelling (indirect) effect of the storm-time equatorward neutral wind (e.g., Richmond and Roble, 1979) that makes the thermosphere richer in molecular [N_2] concentration and poorer in atomic [O] concentration so that chemical recombination becomes faster than normal (e.g., Rishbeth, 1991; Fuller-Rowell *et al.,* 1994; Prolss, 1995). The causes of positive ionospheric storms are also beginning to be understood (e.g., Reddy *et al.,* 1990; Werner *et al.,* 1999; Namgaladze *et al*., 2000; Basu *et al.,* 2001; Balan *et al.,* 2003).

Kelley *et al*. (2004) suggested that the plasma's root origin for the positive ionospheric storms at low-mid latitudes lies in the fully sunlit equatorial ionosphere where a penetrating eastward electric field (PEEF) strengthens the daytime equatorial plasma fountain (Hanson and Moffett, 1966; Balan and Bailey, 1995) to a super plasma fountain. The penetrating electric field drives the plasma upward so that it cannot recombine. This plasma spills over the equatorial ionisation anomaly (EIA) (Namba and Maeda, 1939; Appleton, 1946; Anderson, 1973; Watanabe *et al.,* 1995; Huba *et al.,* 2000) and then is driven poleward by a penetrating zonal electric field (Kelley *et al.,* 2004). Tsurutani *et al*. (2004) and Mannucci *et al*. (2005) also follow the super plasma fountain approach to discuss the positive ionospheric storms observed in total electron content (TEC) during the October 2003 super storms. Saito and Araki (2006) report DMSP (Defence Meteorological Satellite Programs) F15 satellite observations of dayside oxygen ion uplift to ≈840 km altitude during the October 30, 2003 super storm. Recently, Lin *et al*. (2005) presented modeling studies of the relative importance of the electric field and neutral wind in leading to the positive ionospheric storms in TEC. Their results suggest that, in addition to the penetrating electric field, the storm-time equatorward neutral wind is important in producing positive storms in N_{max} and TEC. Maruyama *et al*. (2007) suggest that disturbance dynamo electric field and storm-time equatorward surge are important in expanding intense ionospheric storms to lower mid latitudes.

Though Kelley *et al*. (2004) suggested that PEEF could be the root cause of positive ionospheric storms, the suggestion does not seem to consider the effects of diffusion and neutral wind. In this paper we present the relative importance of the PEEF and equatorward neutral wind on positive ionospheric storms at low-mid latitudes. The observations presented in Section 3 show positive ionospheric

*On leave from Department of Physics, University of Kerala, India.

storms in TEC and N_{max} in Japan longitudes during the rare super double geomagnetic storm during 07–11 November 2004, described in Section 2. The relative importance of PEEF and direct effects of equatorward wind on positive ionospheric storms are studied using the Sheffield University Plasmashpere Ionosphere Model (SUPIM) (Bailey and Balan, 1996) in Section 4. The discussions in Section 5 contain the possible main drivers of the positive ionospheric storms (in N_{max}) around the equator. No quantitative data/model comparisons are attempted because the model (SUPIM), though a good tool for studying the relative importance of the drivers, cannot account for the actual temporal and spatial variations of the drivers present during the storm period.

2. Geomagnetic Storm

Figure 1 shows the geomagnetic storm indices (K_p and D_{st}) and the dynamic pressure (panel 1) of the extreme solar wind (or coronal mass ejection CME) that produced the storm. The X-component of the magnetic field (one-minute resolution) at a low latitude station is also shown (panel 2) for comparison. The geomagnetic data are obtained from the World Data Center in Kyoto, and solar wind data are from ACE (Advanced Composition Explorer) spacecraft (Skoug *et al*., 2004). As shown by Fig. 1, while ring current was trying to develop (decrease in X-component) after the compression of magnetopause (increase in X-component) by the first CME pulse, the next CME pulse compressed the magnetopause. This process repeated at the arrival of the successive CME pulses (top panel) ultimately resulted in the rare super double geomagnetic storm, with three positive initial phases (numbered 1, 2 and 3 in panel 4). The CME clouds during 07–08 November produced the first super storm, with storm sudden commencement (SSC) at 02:53 UT and storm main phase (MP1) onset at ≈21:30 UT on 07 November; D_{st} reached −373 nT at 07:00 UT and K_p reached 9 during 03:00–09:00 UT on 08 November. While the storm was recovering, the next CME clouds during 09–11 November reintensified the storm, with second MP (MP2) onset at ≈12:00 UT on 09 November; D_{st} reached −289 nT at 11:00 UT and K_p reached 9 during 09:00–12:00 UT on 10 November.

3. Ionospheric Storm

The ionospheric responses to the geomagnetic storms (Fig. 1) are shown in Figs. 2 and 3. Figure 2 shows the GPS-TEC obtained using the GPS receiver network (over 1000 GPS receivers) in Japan. The phase delays and Pseudoranges of the GPS signals recorded by the network are used to derive absolute vertical TEC with a time resolution of 30 seconds and spatial resolution of 0.15°. The instrument biases inherent in the receivers and transmitters are taken care of by using a least square fitting method (Otsuka *et al.,* 2002). In Fig. 2, solid curves show the TEC variations during the storm period (07–11 November 2004) at four locations (20°N mag. lat., 130°E; 25°N, 135°E; 30°N, 142°E; 35°N, 142°E), and dotted curves give the corresponding average TEC during the seven quiet days (31 October–06

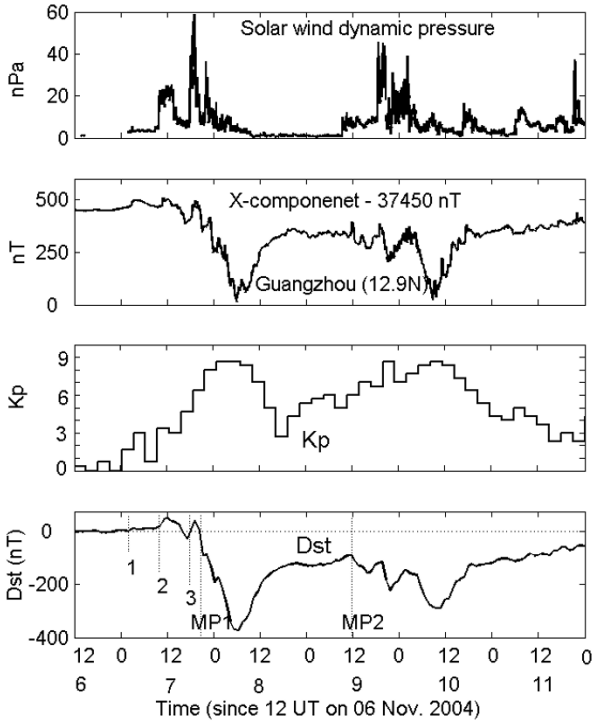

Fig. 1. Comparison of the rare super double geomagnetic storm indices (D_{st} and K_p) with the solar wind dynamic pressure (top panel). The X-component (minus 37450 nT) of the geomagnetic field at a low latitude station (Guangzhou, 23.1°N 113.3°E, 12.9°N mag. lat.) is also shown for comparison.

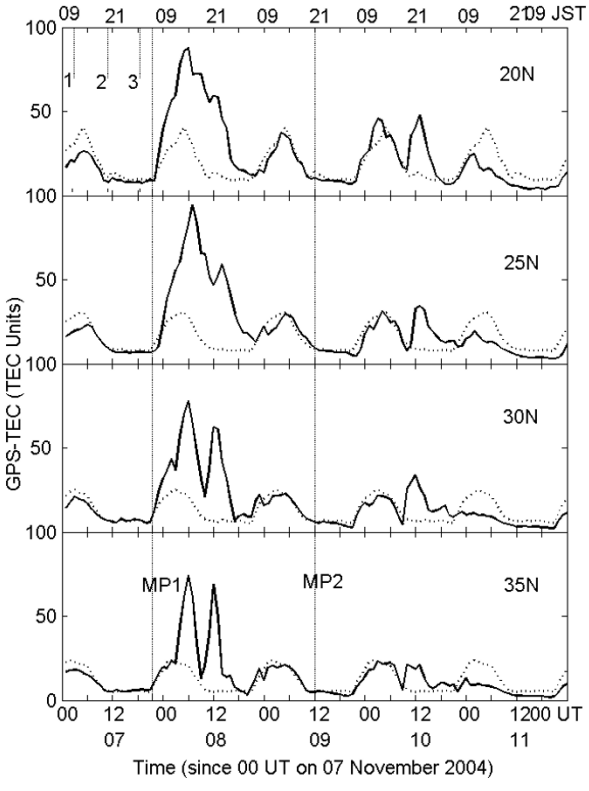

Fig. 2. Comparison of GPS-TEC in 20–35°N magnetic latitudes in Japan during 07–11 November 2004 (solid curves) with the average TEC (dotted curve) during the seven quiet days prior to the geomagnetic storm (31 October–06 November 2004). The local time (or JST) is noted at the top.

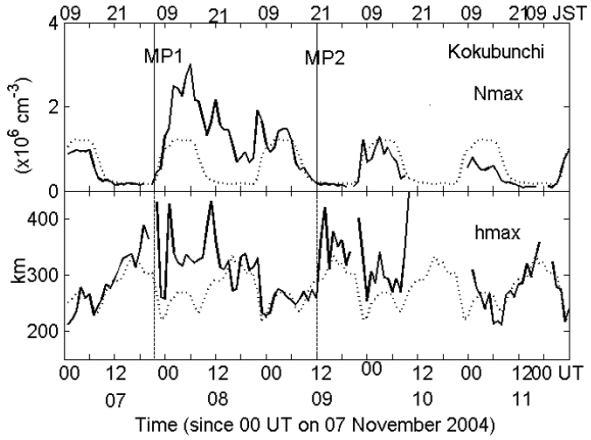

Fig. 3. Comparison of peak electron density (N_{max}) and peak height (h_{max}) at a typical mid latitude station Kokubunji (35.7°N, 139.5°E; 26.8°N geomag. lat.) in Japan during 07–11 November 2004 (solid curves) with the average N_{max} and h_{max} (dotted curves) during the seven quiet days prior to the geomagnetic storm (31 October–06 November 2004). The local time (or JST) is noted at the top.

November) prior to the storm. For Fig. 2, the TEC within $1.05^\circ \times 1.05^\circ$ latitude-longitude grid at four locations are averaged for each hour. The numbers 1, 2 and 3 in the top panel correspond to the times of onset of the positive initial phases. The main phase onsets (MP1 and MP2, noted by vertical lines) occurred at around sunrise (≈06:30 LT) and evening (≈21:00 LT).

As shown by Fig. 2, the response of the low-mid latitude ionosphere to the first geomagnetic storm is a strong positive ionospheric storm. Following the onset of the main phase (MP1) at around sunrise (06:30 LT) on 08 November, TEC increased by up to three times. The peak electron density (N_{max}) and peak height (h_{max}) also showed similar positive ionospheric responses at these low-mid latitudes. Figure 3 shows the N_{max} and h_{max} variations at a typical lower mid latitude station Kokubunji (35.7°N, 139.5°E; 26.8°N geomag. lat.) where N_{max} increased by up to three times and h_{max} increased by over 150 km on 08 November. The second geomagnetic storm with MP2 onset in the evening (21:00 LT) on 09 November is expected to produce a negative ionospheric storm on the following day (e.g., Rishbeth, 1991; Prolss, 1995). However, no significant changes in TEC and N_{max} are observed (Figs. 2 and 3), maybe because the effects of the second geomagnetic storm are embedded in those of the first storm. However, relatively small increase in TEC (and N_{max}) followed by a large increase in h_{max} (Fig. 3) occurred after sunset on 10 November.

Though the initial phases of the geomagnetic storm lasted for about 18 hours (numbers 1, 2 and 3, Figs. 1 and 2), no significant changes occurred in TEC and N_{max} at low-mid latitudes during this period (Figs. 2 and 3). However, the high latitude ionosphere as observed by the EISCAT radar (results not shown) responded directly to the changes in the dynamic pressure of the CMEs that produced the initial phases. These results confirm that CMEs cannot directly affect the low-mid latitude ionosphere due to closed field lines (shielding effect), and penetrating electric field was absent during the initial phases (Section 5.1). Unlike TEC and N_{max}, h_{max} started increasing well before MP1 onset (Fig. 3). This indicates that the equatorward surge (or travelling atmospheric disturbances, TADs) and equatorward meridional neutral wind produced by high latitude heating (e.g., Richmond and Roble, 1979; Fuller-Rowell *et al.*, 1994) could have reached the low-mid latitude regions before MP1 onset. However, the wind could only raise the ionosphere in altitude and could not assist in increasing TEC and N_{max} because it was mainly dark before MP1 onset. The storm-time increase in TEC (and N_{max}) at 35°N is delayed compared to lower latitudes (Fig. 2), and there are large fluctuations in TEC (and N_{max}) especially at higher latitudes (30°N and 35°N, Fig. 2). Such features have been observed earlier and attributed to the fluctuations in neutral wind (e.g., Sahai *et al.*, 2004).

4. Penetrating Electric Field

The strongest ever recorded prompt penetration electric field was observed during this geomagnetic storm at the equatorial station Jicamarca (Fejer *et al.,* 2007). Figure 4 (bottom panel, solid curve) shows the vertical $\mathbf{E}\times\mathbf{B}$ plasma drift velocity measured at Jicamarca (11.9°S, 76.8°W; dip latitude 1°N) during 09–10 November; data are available only from 09 November. The dotted curve gives the corresponding quiet-time average drift velocity. As shown, the

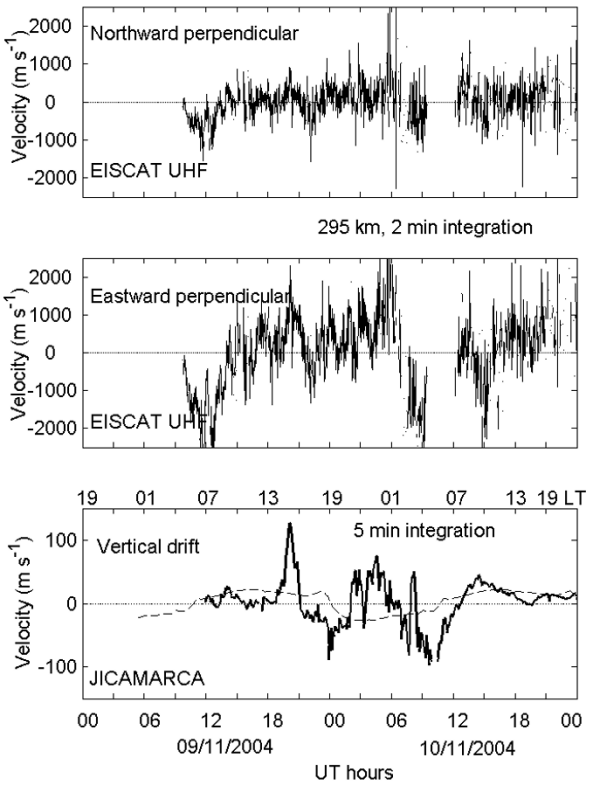

Fig. 4. Comparison of the vertical $\mathbf{E}\times\mathbf{B}$ drift velocity measured at the equatorial station Jicamarca (integrated for five minutes intervals and over ≈200–600 km altitudes) during 09–10 November 2004 (solid curve, bottom panel) with the average quiet-time drift velocity during the time of the year (dashed curve). Top panels give the corresponding northward and eastward perpendicular ion drift velocities (integrated for two minutes intervals) at 295 km altitude at high latitudes measured by the EISCAT radar. The data are available only from 09 November.

velocity during the storm period undergoes large deviations from the average velocity, and the strongest upward drift (or eastward electric field) occurred for about two hours at around 20:00 UT. The top two panels of Fig. 4 show the north-south and east-west plasma drift velocities measured at high latitudes by the EISCAT radar (69.6°N, 19.2°E). As shown by the comparison, the strongest eastward electric field at Jicamarca coincides with a strong and clear peak in the high latitude electric field, suggesting prompt penetration. The direction of IMF (interplanetary magnetic field) was also found to be suitable for the penetration to occur (Kikuchi *et al.,* 2000); IMF B_z (not shown) turned strongly negative for about two hours centered at 20:00 UT. The phase of the geomagnetic storm (main phase of the second storm) was also suitable for the penetration. The upward drift corresponding to the prompt penetration eastward electric field measured at Jicamarca at around 20:00 UT on 09 November (Fig. 4, bottom panel) will be used in assessing the effects of penetrating electric field on positive ionospheric storms in Japan longitude. The other unusually large deviations of the vertical drift observed at Jicamarca during 09–10 November 2004 (Fig. 4, bottom panel) are also discussed by Fejer *et al*. (2007), and seem to be due to eastward and westward prompt penetration and disturbance dynamo action (e.g., Blanc and Richmond, 1980; Kikuchi *et al.,* 2000).

5. Model Results

The SUPIM model (Bailey and Balan, 1996) is used in the model calculations following the procedure described by Balan and Bailey (1995). The model solves the coupled time-dependent equations of continuity, momentum, and energy for the electrons and ions (O^+, H^+, He^+, N_2^+, NO^+, and O_2^+) using the implicit finite-difference method along closed eccentric-dipole geomagnetic field lines. For this study, 200 field lines with apex altitude distributed from 150 km to 12000 km are used for the Japan longitude (135°E) for the day of observation (312) under medium solar activity ($F_{10.7} = 105$). In the calculation of the plasma $\mathbf{E}\times\mathbf{B}$ drift, SUPIM uses a semi-Lagrangian method that follows field lines to move vertically and horizontally with the $\mathbf{E}\times\mathbf{B}$ drifts and interpolates back to a fixed coordinate at each time step.

The vertical $\mathbf{E}\times\mathbf{B}$ drifts measured at Jicamarca (Fejer *et al*., 1991, 2007), with and without PEEF (Fig. 5(a)), are used in the calculations and are applied to all field lines (all apex altitudes from 150 to 12000 km). The neutral wind velocities are from the horizontal wind model (HWM90, Hedin *et al*., 1991) and neutral densities are from MSIS86 (Hedin, 1987). HWM90 and MSIS86 provide neutral wind velocities and densities as function of altitude, latitude, longitude and local time. The Jicamarca quiet-time drift, and HMW90 quiet-time ($A_p = 4$) wind and their modifications (for magnetically active conditions) are used in the calculations because measured values of these parameters are not available for the Japan longitude. Figure 5(a) (top panels) shows the $\mathbf{E}\times\mathbf{B}$ drifts and samples of the effective meridional neutral winds used in the calculations. The quiet-time ($A_p = 4$) neutral densities (MSIS-86) are used in all calculations because the study does not consider the indirect effects

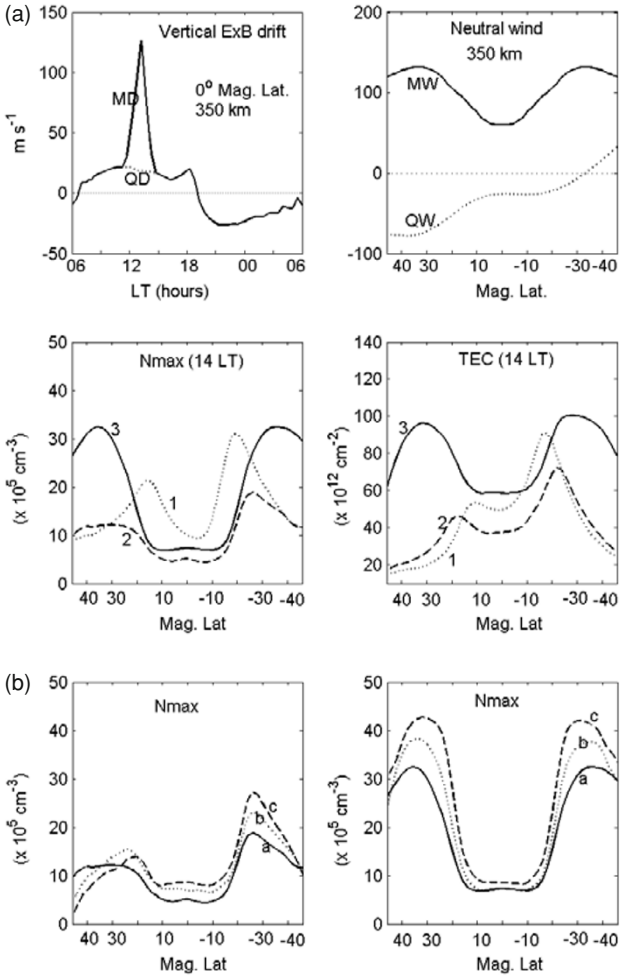

Fig. 5. (a) Top panels—Local time variations of quiet-time (QD) and modified (MD) $\mathbf{E}\times\mathbf{B}$ drifts at the geomagnetic equator at 350 km altitude (top left); MD incorporates PEEF at around 14:00 LT (05:00 UT). Top right shows sample latitude variations of the quiet-time (QW) and modified (MW) effective meridional neutral wind velocities (positive equatorward) at 14:00 LT at 350 km altitude (from HWM90). Bottom panels—Latitude variations at 14:00 LT (05:00 UT) of model N_{max} and TEC obtained with $\mathbf{E}\times\mathbf{B}$ drift (QD) and neutral wind (QW) (dotted curves 1), with $\mathbf{E}\times\mathbf{B}$ drift (MD) and neutral wind (QW) (dashed curves 2), and with $\mathbf{E}\times\mathbf{B}$ drift (MD) and neutral wind (MW) (solid curves 3). (b) Latitude variations at 14:00, 15:00 and 16:00 LT (05:00, 06:00 and 07:00 UT) (curves a, b and c) of model N_{max} obtained with $\mathbf{E}\times\mathbf{B}$ drift (MD) and neutral wind (QW) (left hand panel), and with $\mathbf{E}\times\mathbf{B}$ drift (MD) and neutral wind (MW) (right hand panel).

of neutral wind (or changes in thermospheric composition).

5.1 Effects of PEEF

Two sets of calculations are carried out to assess the effects of PEEF, first set (1) the with quiet-time $\mathbf{E}\times\mathbf{B}$ drift (QD, Fig. 5(a), top left) and second set (2) with a modified $\mathbf{E}\times\mathbf{B}$ drift (MD, Fig. 5(a), top left) that incorporates the strong PEEF observed at Jicamarca into the quiet-time drift at around 14:00 LT. Both sets of calculations (1) and (2) use quiet-time ($A_p = 4$) neutral wind (sample QW, Fig. 5(a), top right). The curves 1 and 2 in the bottom panels of Fig. 5(a) show the latitude variations of the model N_{max} and TEC (integrated up to 1800 km altitudes) at 14:00 LT obtained from the calculations (1) and (2); 14:00 LT falls near the peak of PEEF and diurnal maxima in N_{max} and TEC. A comparison of curves 1 (dotted) and 2 (dashed) show that

the PEEF (or super plasma fountain) shifts the EIA crests in N_{max} and TEC (curves 2) to higher than normal latitudes and reduces their values at latitudes at and within the crests, and there are small increases in TEC at latitudes poleward of the crests; the poleward shift of the EIA crest (up to about 15 degrees) is also larger in the (northern) hemisphere of stronger poleward wind as expected (Balan and Bailey, 1995). In other words, as shown by curves 1 and 2, the PEEF on its own is unlikely to produce positive ionospheric storms at low-mid latitudes. These effects are expected because the daytime upward $\mathbf{E}\times\mathbf{B}$ drift (or eastward electric field) produces the EIA in N_{max} and TEC mainly by generating the trough, which becomes deeper and wider for stronger (penetrating) eastward electric field.

The daytime upward $\mathbf{E}\times\mathbf{B}$ drift drives the plasma vertically upward over the geomagnetic equator (Martyn, 1955), and plasma velocity turns poleward at higher latitudes due to the inclination of the field lines and diffusion along the field lines due to gravity (Mitra, 1946). The net effect of the plasma fountain (Hanson and Moffett, 1966; Balan and Bailey, 1995) combined with daytime production and chemical recombination produces the EIA in N_mF_2 and TEC mainly by generating the trough, and by adding a small amount of plasma poleward of the crests in the topside ionosphere. The curves 1 and 2 (Fig. 5(a)) also illustrate the effects of quite-time neutral wind. The wind makes the EIA crest stronger in the hemisphere of equatorward wind (or less poleward wind) though the plasma velocity turns more poleward in the hemisphere of poleward wind (e.g., Anderson, 1973; Balan and Bailey, 1995). An additional layer also occurs around the equator (Balan *et al.*, 1998), which becomes strong during PEEF (studied in another paper).

5.2 Effects of neutral wind

During geomagnetic storms, the daytime neutral wind can become equatorward due to the additional high latitude heating (e.g., Richmond and Roble, 1979; Fuller-Rowell *et al.*, 1994). The storm-time equatorward wind can affect the ionosphere through its indirect and direct effects. The indirect (upwelling and downwelling) effects of the equatorward wind, which involve changes in thermospheric composition, will be discussed in Section 6. The direct effects of the wind do not involve changes in thermospheric composition but reduce poleward plasma flow (along geomagnetic field lines) and raise the ionosphere to high altitudes of reduced chemical loss. These direct effects of the equatorward wind with and without PEEF (or equivalently strong eastward electric fields due to disturbance dynamo) are modeled in this section (5.2).

The equatorward wind is obtained from the quite-time ($A_p = 4$) HWM90 wind. The meridional component of the quiet-time wind (sample QW, Fig. 5(a), top right) during daytime (06:00–18:00 LT) is multiplied by -2.0 for latitudes $>0^\circ$N and the resulting wind is applied to both northern and southern hemispheres. A sample of the resulting effective equatorward wind (MW) is shown in Fig. 5(a) (top right). It may be noted that the velocity and latitude extent of the equatorward wind are decided mainly by the high latitude energy input during geomagnetic storms (e.g., Richmond and Roble, 1979; Fuller-Rowell *et al.*, 1994). The solid curves 3 in Fig. 5(a) show the latitude variations of N_{max} and TEC obtained from the calculations (3) that use the equatorward neutral wind (MW) and $\mathbf{E}\times\mathbf{B}$ drift (MD) with PEEF.

As shown by the comparison of curves 2 and 3 (Fig. 5(a)), the direct effects of the equatorward wind in the presence of daytime PEEF can increase N_{max} at latitudes greater than about $\pm15^\circ$; the large depletion within $\pm15^\circ$ is due to PEEF. However, TEC (curve 3) increases above the quiet-time level (curve 1) at all latitudes except for a narrow region in the south. These results (curves 3, Fig. 5(a)) indicate that the PEEF can cause positive ionospheric storms in TEC at low-mid latitudes as suggested by Kelley *et al.* (2004) but only in the presence of an equatorward wind. With the equatorward wind, N_{max} can also show positive storms though not around the equator.

It is known that the plasma takes some time to redistribute themselves after being lifted to high altitudes by the strong upward $\mathbf{E}\times\mathbf{B}$ drift. So it becomes interesting to see how the EIA structure changes with time after the peak of the $\mathbf{E}\times\mathbf{B}$ drift. That is illustrated in Fig. 5(b), which shows the latitude variation of N_{max} at 14:00, 15:00 and 16:00 LT (curves a, b and c); left hand panel obtained with drift MD and wind QW (calculations 2) and right hand panel obtained with drift MD and wind MW (calculations 3); N_{max} alone is shown for simplicity. As shown, the EIA structure remains similar during 14:00–16:00 LT. However, the EIA crest becomes stronger and moves equatorward (right hand panel) as expected from the effect of the equatorward wind. The crest in the left hand panel also becomes stronger with time during 14:00–16:00 LT in the southern hemisphere of weaker poleward wind (see also Fig. 5(a), top right).

Positive ionospheric storms can also occur without PEEF. The calculations (3) are therefore repeated without PEEF. These calculations (4) use the same equatorward wind (sample MW, Fig. 5(a), top right) as calculations (3) but use the quiet-time $\mathbf{E}\times\mathbf{B}$ drift QD (Fig. 5(a), top left) instead of the drift MD with PEEF. The solid curves 4 in Fig. 6 show the latitude variations of N_{max} and TEC obtained from the calculations (4). The curves 3 (dashed) from calculations (3) and curves 1 (dotted) from calculations (1) are also reproduced in Fig. 6 for comparison. The results in Fig. 6 show that the direct effects of the storm-time equatorward wind can produce stronger positive iono-

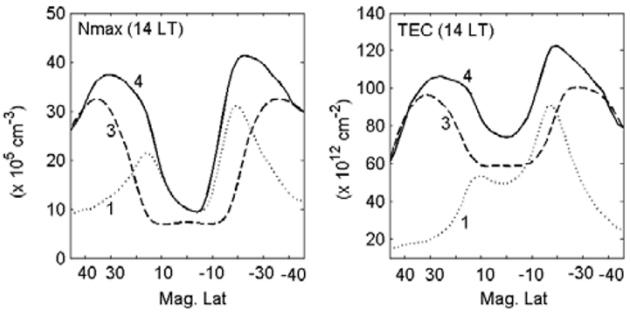

Fig. 6. Latitude variations at 14:00 LT (05:00 UT) of model N_{max} and TEC (solid curves 4) obtained using the quiet-time $\mathbf{E}\times\mathbf{B}$ drift QD (Fig. 5(a), top left) and equatorward neutral wind MW (Fig. 5(a), top right). Curves 3 (dashed) and curves 1 (dotted) are reproduced from Fig. 5(a) for comparison.

spheric storms without PEEF (curves 4) than with PEEF (curves 3) in both N_{max} and TEC at all low-mid latitudes except in N_{max} around the equator. N_{max} around the equator (curve 4) does not rise above the quiet-time level (curve 1) because the horizontal wind cannot affect N_{max} at the geomagnetic equator where the geomagnetic field is also horizontal.

6. Discussion

The results presented above have shown that the direct effects of the equatorward neutral wind can be the main driver of positive ionospheric storms in N_{max} and TEC at low-mid latitudes except in N_{max} around the equator. The direct effects of the wind can also result in stronger positive ionospheric storms without PEEF (or strong eastward electric field of dynamo origin) than with PEEF. The PEEF can also cause positive ionospheric storms (except in N_{max} around the equator) but only in the presence of an equatorward wind.

The indirect (downwelling) effect of the equatorward wind can make the low latitude thermosphere richer in atomic concentration ([O]) and poorer in molecular concentration ([N_2]) (e.g., Richmond and Roble, 1979) as observed by GUVI. This indirect effect of the wind can contribute to daytime positive ionospheric storms at low latitudes (including N_{max} around the equator) through enhanced production of ionisation. On the other hand, the indirect (upwelling) effect of the wind, as mentioned in Section 1, can cause negative ionospheric storms at mid latitudes (e.g., Rishbeth, 1991; Fuller-Rowell *et al.,* 1994; Prolss, 1995). The net effect of all the main drivers (electric fields, and direct and indirect effects of neutral wind) can produce positive ionospheric storms at low-mid latitudes if the main phase of the geomagnetic storm occurs in the morning-noon local time (e.g., Lin *et al.,* 2005) when production of ionisation dominates over chemical loss of ionisation as observed in the present case (Figs. 2 and 3). However, quantitative data/model comparisons are beyond the scope of this study for the reasons mentioned in Section 1.

Though Kelley *et al*. (2004) suggested that the daytime PEEF can be the root cause of positive ionospheric storms (in TEC) at low-mid latitudes, the model results in this paper show that the suggestion can work only in the presence of an equatorward wind. That is because to produce positive ionospheric storms, the plasma raised to higher than normal altitudes and latitudes by the strong $\mathbf{E}\times\mathbf{B}$ (or PEEF) should not be allowed to get lost by heavy chemical loss at low altitudes; in other words, the downward flow velocity component (along field lines) due to diffusion (or gravity) should be reduced or stopped. An equatorward neutral wind does this and also raises the ionosphere to high altitudes of reduced chemical loss. For these reasons, if a strong eastward penetration occurs in the presence of an adequate equatorward neutral wind during daytime (preferably before noon), there can be a strong positive ionospheric storm. Tusrutani *et al*. (2004) and his colleagues also seem to study such cases. The electron and ion densities in the topside ionosphere also increase during such events as observed at around 840 km altitude by Saito and Araki (2006) during the October 2003 super storm.

7. Conclusion

The relative importance of penetrating eastward electric field (PEEF) and direct effects of storm-time equatorward neutral wind on positive ionospheric storms at low-mid latitudes are studied using observations and modeling. The study during the super storm of 08 November 2004 shows that the direct effects of storm-time equatorward wind (that reduce poleward plasma flow and raise the ionosphere to high altitudes of reduced chemical loss) can be main driver of positive ionospheric storms at low-mid latitudes except in N_{max} around the equator. PEEF on its own is unlikely to produce positive ionospheric storms. However, PEEF can lead to positive ionospheric storms in the presence of an equatorward wind.

Acknowledgments. We acknowledge the WDC for ionosphere, Tokyo, National Institute of Information and Communications Technology (Japan) for providing the ionosonde data. We also thank the ACE SWEPAM instrument team and ACE Science Center for providing the ACE data, and WDC (Kyoto) for providing the geomagnetic data. Vijaya Lekshmi thanks UGC (India) for providing a fellowship under the FIP scheme. The work at Sheffield is supported by PPARC (UK) grant No. PPA/G/S/1999/00705.

References

Abdu, M. A., Major phenomena of the equatorial ionosphere-thermosphere system under disturbed conditions, *J. Atmos. Sol. Terr. Phys*., **59**(13), 1505, 1997.

Anderson, D. N., A theoretical study of the ionospheric F region equatorial anomaly, I, Theory, *Planet. Space Sci*., **21**, 409, 1973.

Appleton, E. V., Two anomalies in the ionosphere, *Nature*, **157**, 691, 1946.

Bailey, G. J. and N. Balan, A low latitude ionosphere-plasmasphere model, in *STEP Hand Book of ionospheric models*, edited by R. W. Schunk, p.173, Utah State University, Logan, UT 84322–4405, 1996.

Balan, N. and G. J. Bailey, Equatorial plasma fountain and its effects—possibility of an additional layer, *J. Geophys. Res*., **100**, 21421, 1995.

Balan, N. and P. B. Rao, Dependence of ionospheric response on the local time of sudden commencement and intensity of geomagnetic storms, *J. Atoms. Terr. Phys*., **52**, 269, 1990.

Balan, N., I. S. Batista, M. A. Abdu, J. Macdougall, and G. J. Bailey, Physical mechanism and statistics of occurrence of an additional layer in the equatorial ionosphere, *J. Geophys. Res*., **103**, 29169, 1998.

Balan, N., *et al*., Simultaneous mesosphere/lower thermosphere and thermospheric F region observations during geomagnetic storms, *J. Geophys. Res*., **109**, A04308, doi.:10.1029/2003JA009982, 2003.

Basu, S., Sa. Basu, K. M. Groves, H. C. Yeh, F. J. Rich, P. J. Sultan, and M. J. Keskinen, Response of the equatorial ionosphere to the great magnetic storm of July 15, 2000, *Geophys. Res. Lett*., **28**(18), 3577, 2001.

Blanc, M. and A. D. Richmond, the ionospheric disturbance dynamo, *J. Geophys. Res*., **85**, 1669, 1980.

Fejer, B. G., E. R. Depaula, S. A. Gonzales, and R. F. Woodman, Average vertical and zonal F region plasma drifts over Jicamarca, *J. Geophys. Res*., **96**, 13901, 1991.

Fejer, B. G., J. W. Jensen, T. Kikuchi, M. A. Abdu, and J. L. Chau, Equatorial ionospheric electric fields during the November 2004 magnetic storm, *J. Geophys. Res*., 2007 (in press).

Fuller-Rowell, T. J., M. V. Codrescu, R. J. Moffett, and S. Quegan, Response of the thermosphere and ionosphere to geomagnetic storms, *J. Geophys. Res*., **99**, 3893, 1994.

Hanson, W. B. and R. J. Moffett, Ionisation transport effects in the equatorial F region, *J. Geophys. Res*., **71**, 5559, 1966.

Hedin, A. E., MSIS-86 thermospheric model, *J. Geophys. Res*., **92**, 4649, 1987.

Hedin, A. E., *et al*., Revised global model of thermosphere winds using satellite and ground-based observations, *J. Geophys. Res*., **96**, 7657, 1991.

Huba, J. D., G. Joyce, and J. A. Fedder, Semi2 is another model of the ionosphere (SAMI2): A new low-latitude ionosphere model, *J. Geophys. Res*., **105**, 23035, 2000.

Kelley, M. C., M. N. Vlasov, J. C. Foster, and A. J. Coster, A quantita-

tive explanation for the phenomenon known as torm-enhanced density, *Geophys. Res. Lett.*, **31**, L19809, doi:10.1029/2004GL020875, 2004.

Kikuchi, T., H. Luhr, K. Schlegel, H. Tachihara, M. Shinohara, and T.-I. Kitamura, Penetration of auroral electric fields to the equator during a substorm, *J. Geophys. Res.*, **105**, 23251, 2000.

Lin, C. H., A. D. Richmond, R. A. Heelis, G. J. Bailey, G. Lu, J. Y. Liu, H. C. Yeh, and S. Y. Su, Theoretical study of the low and mid latitude ionospheric electron density enhancement during the October 2003 super storm: Relative importance of the neutral wind and the electric field, *J. Geophys. Res.*, **110**, A12312, doi:10.1029/2005JA011304, 2005.

Mannucci, A. J., B. T. Tsurutani, B. A. Iijima, A. Komjathy, A. Saito, W. D. Gonzalez, F. L. Guarnieri, J. U. Kozyra, and R. Skoug, Dayside global ionospheric response to the major interplanetary events of October 29–30, 2003 "Halloween Storms", *Geophys. Res. Lett.*, **32**, L12S02, doi:10.1029/2004GL021467, 2005.

Martyn, D. F., Theory of height and ionisation density changes at the maximum of a Chapman-like region, taking account of ion production, decay, diffusion and total drift, *Proceedings Cambridge Conference*, p.254, Physical Society, London, 1955.

Maruyama, T. and M. Nakamura, Conditions for intense ionospheric storms expanding to lower mid latitudes, *J. Geophys. Res.*, **112**, A05310, doi:10.1029/2006JA012226, 2007.

Matsushita, S., A study of the morphology of ionospheric storms, *J. Geophys. Res.*, **13**, 305–321, 1959.

Matuura, N., Theoretical models of ionospheric storms, *Space Sci. Rev.*, **13**, 124–189, 1972.

Mitra, S. K., Geomagnetic control of region F_2 of the ionosphere, *Nature*, **158**, 668, 1946.

Namba, S. and K.-I. Maeda, *Radio Wave Propagation*, 86pp., Corona, Tokyo, 1939.

Namgaladze, A. A., M. Forster, and R. Y. Yurik, Analysis of the positive ionospheric response to a moderate geomagnetic storm using a global numerical model, *Ann. Geophys.*, **18**, 461–477, 2000.

Otsuka, Y., *et al.*, A new technique for mapping of total electron content using GPS netwrok in Japan, *Earth Planets Space*, **54**, 63–70, 2002.

Prolss, G. W., Ionospheric F region storms, in *Handbook of Atmospheric Electrodynamics*, edited by H. Volland, 195–248, CRC Press, Boca Raton, 1995.

Reddy, C. A., S. Fukao, T. Takami, M. Yamamoto, T. Tsuda, T. Nakamura, and S. Kato, A MU Radar-based study of mid-latitude *F* region response to a geomagnetic disturbance, *J. Geophys. Res.*, **95**, 21,077, 1990.

Richmond, A. D. and R. G. Roble, Dynamic effects of aurora-generated gravity waves on the mid-latitude ionosphere, *J. Atmos. Terr. Phys.*, **41**, 841, 1979.

Rishbeth, H., F-region storms and thermospheric dynamics, *J. Geomag. Geoelectr.*, **43**, 513, 1991.

Sahai, Y., P. R. Fagundes, and F. Becker-Guedes, Longitudinal differences observed in the ionospheric F-region during the major geomagnetic storm of 31 march 2001, *Ann. Geophys.*, **22**(9), 3221, 2004.

Saito, A. and T. Araki, DMSP observation of dayside oxygen ion uplift to 840 km altitude during the October 30, 2003 magnetic super storm, *Geophys. Res. Lett.,* 2006 (submitted).

Skoug, R. M., J. T. Gosling, J. T. Steinberg, D. J. McComas, C. W. Smith, N. F. Ness, Q. Hu, and L. F. Burlaga, Extremely high speed solar wind: October 29–30, 2003, *J. Geophys. Res.*, **109**, A09102, doi:10.1029/2004JA010494, 2004.

Tsurutani, B., *et al.*, Global dayside ionospheric uplift and enhancement associated with interplanetary electric fields, *J. Geophys. Res.*, **109**, A08302, doi:10.1029/2003JA010342, 2004.

Watanabe, S., K.-I. Oyama, and M. A. Abdu, Computer simulation of electron and ion densities and temperatures in the equatorial F region and comparison with Hinotori results, *J. Geophys. Res.*, **100**, 14581, doi:10.1029/95JA01356, 1995.

Werner, S., R. Bauske, and G. W. Prolss, On the origin of positive ionospheric storms, *Adv. Space Res.*, **24**, 1485–1489, 1999.

N. Balan (e-mail: B.NANAN@sheffield.ac.uk), H. Alleyne, Y. Otsuka, D. Vijaya Lekshmi, B. G. Fejer, and I. McCrea